Excitation of Surface Deformation Modes of a Phase-Separating Polymer Blend on a Patterned Substrate

Giovanni Nisato,* Brett D. Ermi, Jack F. Douglas, and Alamgir Karim

Polymers Division, National Institute of Standards and Technology, Gaithersburg, Maryland 20899

Received October 2, 1998; Revised Manuscript Received January 11, 1999

ABSTRACT: The phase separation kinetics of ultrathin deuterated poly(styrene)/poly(butadiene) polymer blend films spun cast onto striped self-assembled monolayer (SAM) substrates is studied by atomic force microscopy (AFM). Fourier transform analysis of the AFM topographic data at various stages of the film pattern development reveals the presence of quantized surface deformation modes. These modes are excited by the phase separation process when the scale of phase separation becomes commensurate with the period of the striped surface pattern. Thus, higher frequency modes become excited at early stages of phase separation, and these excitations decay with time as the phase separation pattern further coarsens. The film ultimately self-organizes into a periodic structure in which the fundamental mode has the largest amplitude. The influence of film thickness on the film morphology in this late stage is also investigated. A decrease in the film thickness leads to surface patterns that match those of the SAM substrates with increasing resolution. However, these film patterns break up into droplet arrays along the SAM stripes if the films are made too thin. This phenomenon is attributed to a capillary wave instability.

1. Introduction

The surface structure and properties of thin polymeric films are important for an increasing number of applications.[1−8] The ability to achieve nanometric control of the geometry and properties of such "soft" polymeric materials is crucial. Factors limiting the control of surface structure in polymer films are poorly understood, however, and several experiments have sought to push the limits of spatial resolution in polymer surface patterning. Recent measurements demonstrated the control of surface patterning in thin polymer blend films at a micron level,[9−11] but the ultimate goal of nanofabrication remains elusive. It is clear that progress in this field requires a better understanding of the mechanisms governing surface pattern formation in thin polymer films.

Recent measurements have revealed important physical effects that can have a great influence on the properties and structure of thin polymer films. In relatively thin polymer blend films (thickness $L \approx 1\ \mu$m) there is a tendency for the surface to induce the development of composition waves transverse to the solid substrate. In this "surface-directed" spinodal decomposition process, composition waves coarsen with time similarly to bulk phase separation and have been the subject of extensive experimental[12−16] and theoretical[17−21] investigations. A new phenomenon emerges in films thinner than the wavelength of these composition waves. For these ultrathin films ($L < 200$ nm), surface-directed spinodal decomposition is suppressed and phase separation occurs *within* the plane of the film.[22,23]

The experimental study of phase separation in ultrathin films is greatly facilitated by the presence of surface undulations that accompany this type of phase separation.[22−24] Phase separation leads to surface tension variations within the plane of the film, and these modulations in the surface tension induce height variations in the film that can be imaged by atomic force microscopy.[23−25] Recent experiments have shown the presence of bicontinuous spinodal decomposition patterns in near critical ultrathin "symmetric" films, while "bumps" and "holes" are observed in the off-critical polymer blends.[24] These structures disappear when the film is returned to the one-phase region, confirming their phase separation origin.[24]

A variety of experimental methods have been utilized to confirm the existence of phase-separated structures in thin polymer blend films. These include frictional force and compliance atomic force microscopy measurements, scanning secondary ion mass spectroscopy (SIMS), and removal of one of the polymer species by washing the sample with a selective solvent. Some of these techniques have also been applied to blend films on patterned surfaces. We refer the reader to previous work emphasizing the characterization of phase separation in ultrathin films.[11,23,24]

Recent measurements on the dewetting of homopolymer films have indicated another important feature of ultrathin ($L < 100$ nm) polymer films. Capillary wave undulations of the fluid−air interface can lead to film rupture.[26−28] In thicker films ($1\ \mu\text{m} < L < 0.1\ \mu$m), rupturing occurs through the nucleation of holes at random positions within the plane of the film.[29] In thinner films ($L < 10$ nm), a modulated pattern reminiscent of spinodal decomposition forms and this "spinodal dewetting" process ultimately causes the film to break up into droplets having a uniform size and distribution.[30]

Previous studies have established that lateral phase separation and capillary waves have a crucial influence on the properties of thin multiphase polymer films. It seems clear that a *coupling* should exist between these fluctuation phenomena. Theoretical modeling of the coupling between height and composition fluctuations in thin phase-separating films has indicated that the energetic cost of surface deformations arising from composition variations within the film accompanying phase separation can inhibit macroscopic phase separation.[31−36] This can lead to microphase separation in laterally phase-separating fluid mixtures rather than macroscopic phase separation.[31−33,35,36] Previous mea-

10.1021/ma981546x CCC: $18.00
Published on Web 03/10/1999

Table 1. Sample Characteristics

polymer mass fraction (%)[42]	spin cast speed (rpm)	thickness[a] (nm)[45]
3	2000	100
2	2000	60
1	1000	40
1	2000	20

[a] Thicknesses are estimated to within 10%.

surements on phase-separating ultrathin blend films have indeed indicated that the phase separation pattern size becomes stable (i.e., "pinning"[22]) at long times. However, these films do not form the highly ordered patterns found in block copolymer "mesophases".[37] Phase separation patterns having a well-defined scale are seen in lipid mixtures with a free liquid−air boundary. This phenomenon has been suggested to have important biological significance.[34,38]

It is possible to create organized structures in ultrathin polymer blend films by chemically modulating the substrate to guide their organization into regular patterns.[10,11] These techniques exploit the sensitivity of the phase-separating blends to symmetry-breaking perturbations to guide phase separation ("pattern-directed phase separation"). Ordering is expected to occur when the coarsening scale of the composition fluctuations becomes commensurate with the characteristic size of the pattern, leading to a segregation of the two polymer phases to the surface pattern regions that are most energetically favorable.[10]

In the present paper, we study the coupling of surface and composition fluctuations processes through the study of blend phase separation on a stripe-patterned SAM substrate. This geometry is advantageous for our purposes, since the segregation of the polymer components to different regions of the striped substrate leads to a quantization of the surface deformation modes of the free boundary.[39,40] These discrete surface modes can then be separated from the fluctuation spectrum of the phase separation process, allowing us to study their coupling.[41] Our study of the phase separation kinetics on ultrathin films on the patterned substrate reveals a coupling between these modes. The phase separation modes excite the surface modes when the scale of the phase separation pattern becomes commensurate with the scale of the surface undulation modes belonging to the surface patterns. High-frequency modes are first excited as phase separation proceeds, and these excitations decay as coarsening occurs to larger scales. The final morphology is related to the fundamental surface mode of the stripe pattern.

2. Experimental Section

Polymer blend films of dPS ($M_w = 1000$, $M_w/M_n = 1.13$)/PB ($M_w = 5300$, $M_w/M_n = 1.07$)[42] were spun cast from toluene solutions onto self-assembled monolayer (SAM)-covered substrates which contain a stripe pattern over a 1 cm^2 area surrounded by a homogeneous SAM region. The patterned substrates were prepared using the microcontact printing method[43] and consist of alternating stripes of $-CH_3$- and $-$COOH-terminated alkanethiols ($HS(CH_2)_{15}CH_3$ and $HS(CH_2)_{15}$-COOH, respectively). The dPS/PB blend exhibits an upper critical solution temperature of 51 °C and a critical composition of $\phi_{dPS} = 0.70$.[44] Film thickness was varied by adjusting spin-coating speed and polymer concentration, as shown in Table 1. Thicknesses were estimated from X-ray reflectivity data on dPS/PB films cast under similar conditions on silicon substrates.[45]

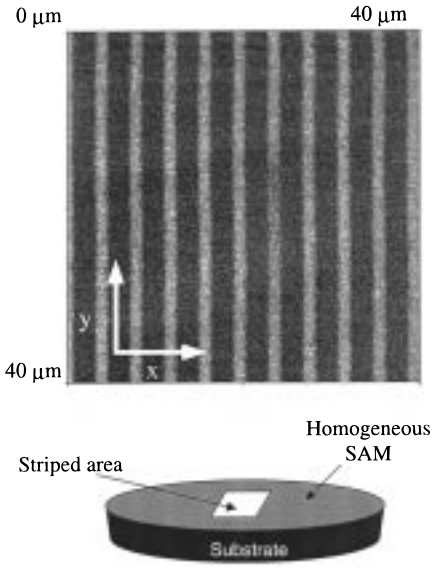

Figure 1. LFM image of the SAM substrate (40 μm × 40 μm). The substrate is topographically flat; bright stripes and dark stripes correspond to $-$COOH- and $-CH_3$-terminated alkanethiols, respectively. The pattern periodicity is 4 ± 0.2 μm. The schematic drawing illustrates the SAM substrates used for this study.

A Topometrix[46] Accurex AFM was used to acquire the topographic images to an estimated vertical resolution of ±1 nm. The AFM experiments were performed using the contact mode, with pyramidal Si_3N_4 tips (Topometrix, contact AFM-1520) supplied by the manufacturer. The nominal force constant of the tip cantilevers was 0.032 N m^{-1}, and forces applied by the tip to the sample were in the range 1−20 nN. All structures shown in the images were reproducible, independent of scan direction or scan range, and collected at a minimum resolution of 400 × 400 pixels.

The SAM substrates were topographically flat, and lateral force microscopy (LFM) measurements were performed to characterize the stripe pattern. Fourier transform of the LFM data yielded a periodicity of 4.0 ± 0.2 μm.[47] An LFM image of the substrate is shown in Figure 1. The x and y axes are defined as the directions transverse to and along the stripe long axis, respectively. On the coated wafer, the SAM patterned areas occupy only a fraction of the total surface of the substrate, so it is possible to compare AFM scans of the blend film phase separation on the patterned versus unpatterned regions.

3. Results and Discussion

The presentation of the results and accompanying discussion is organized as follows: (A) thickness dependence of morphology, (B) time evolution of topography, (C) autocorrelation analysis, and (D) FFT analysis of film patterns.

(A) Thickness Dependence of Morphology. Figure 2 displays a progression of late stage film morphologies for dPS/PB films on SAM patterned substrates for decreasing values of the film thickness (between 100 and 20 nm). The AFM profiles correspond to the final morphology of these thin blend films. The most obvious feature, visible in comparing parts a−c of Figure 2, is the topographical ordering of the film following the symmetry of the underlying pattern. We observe that the alignment of the film structure relative to the SAM stripes becomes increasingly well developed, reaching an apparent maximum alignment for an optimal thickness as depicted in Figure 2c. However, this enhancement in the film pattern alignment and resolution with decreasing film thickness can only be achieved up to a

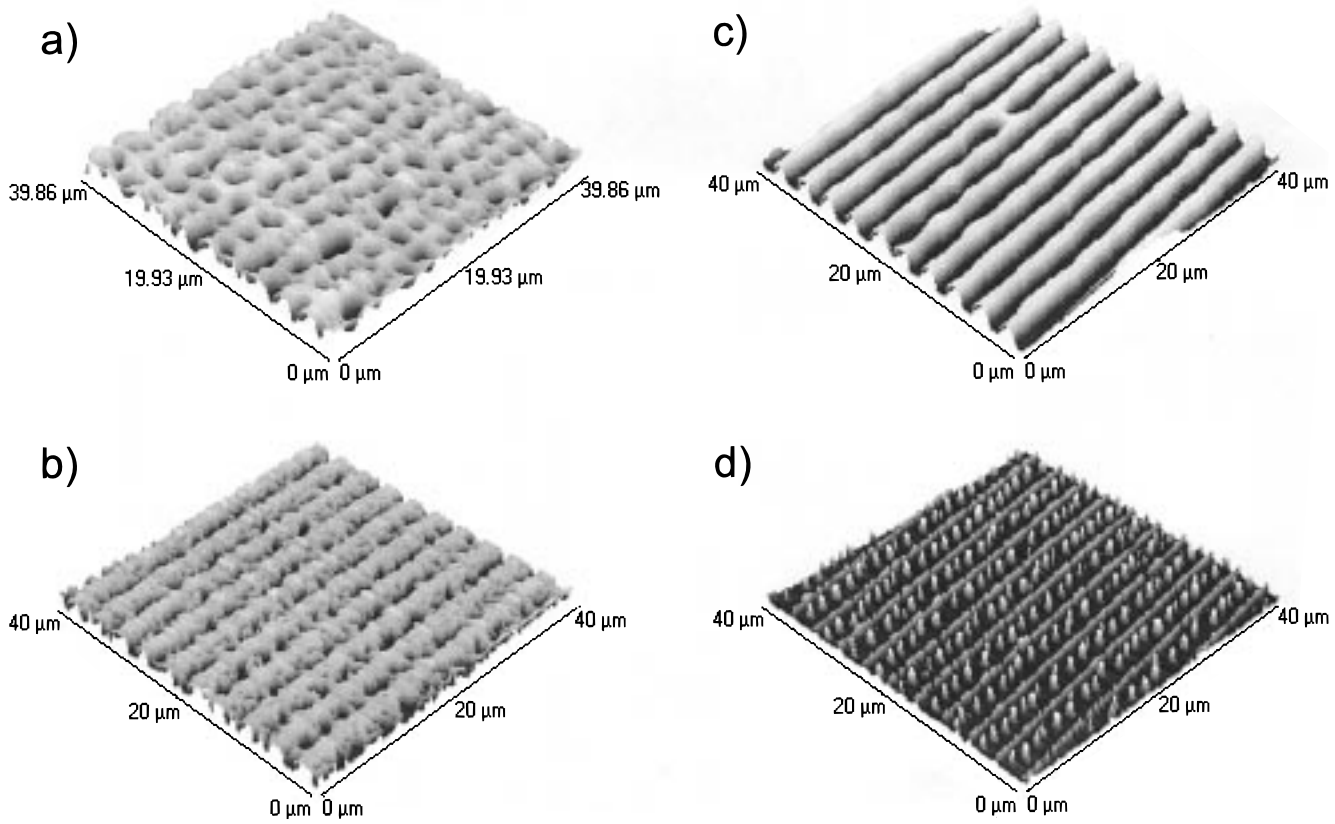

Figure 2. Comparison of film morphologies at the final stage for decreasing film thickness (a) 100, (b) 60, (c) 40, and (d) 20 nm (cf. Table 1). Decreasing thickness induces better overall film ordering corresponding to the spatial modulation of the substrate, until qualitatively different patterns are observed for the thinner sample (d).

point, as illustrated in Figure 2d. In these ultrathin films we observed a tendency of the surface pattern to break up in droplet arrays dispersed rather uniformly on the SAM stripes. The physical origin of this phenomenon will be discussed in section D. The kinetics of the film morphology evolution in the 20 and 40 nm films were too fast for reliable evaluation by AFM. However, the time evolution of the surface patterns in the 60 and 100 nm films were effectively static on the time scale of the measurement, allowing for kinetic studies of film pattern self-organization.

(B) Time Evolution of Topography. The effect of a stripe-patterned SAM substrate on the development of the phase-separating blend films is illustrated in Figure 3. The left column of Figure 3 displays the evolution of a 100 nm thick dPS/PB blend film spun cast on the unpatterned region of the SAM-covered substrate (i.e., homogeneous −COOH-terminated SAM region). These measurements, performed on the same sample, span a time range of 54 h after the film was spin cast. The dark regions correspond to lower and the bright regions correspond to elevated parts of the film. These height variations are caused by the interfacial tension variation accompanying phase separation and have been documented in previous studies.[24] The topography of the same film, but now within the stripe-patterned region of the substrate, is shown in Figure 3d−f for comparable times. Two phenomena are apparent in these images: a coarsening of the spinodal pattern on a finer scale and a long-range ordering with a wavelength corresponding to the SAM pattern periodicity (4 μm). In Figure 4 we show a more complete time series for a thinner (60 nm) sample spun cast on a SAM substrate identical to the one in Figure 3. At intermediate times (e.g., Figure 4c−e) it is possible to discern more complicated topographies, characterized by local maxima in the surface modulation.

Calculation of the mean-averaged profiles as a function of time allows for a direct comparison of the AFM data even when the absolute height is not directly measurable. Averages along the x and y directions are given by $h_y(x) = \langle H(x,y)\rangle_y/\bar{H}$ and $h_x(y) = \langle H(x,y)\rangle_x/\bar{H}$ where $\bar{H}$ is the mean film height; $\langle\,\rangle_x$ and $\langle\,\rangle_y$ represent an average along the x and y directions, respectively. Figure 5 illustrates the line averages corresponding to the AFM data for the 100 nm film on SAM pattern. In the case of the homogeneous substrate (left column, Figure 5a−c), the averages along x and y directions yield similar results since the substrate is isotropic. Since the scan range of the AFM images is held constant, the degree of averaging of the height fluctuations is reduced as the coarsening proceeds. Therefore, the amplitude of the random height fluctuations, visible in Figure 5a−c, increases with time. In the case of the stripe-patterned SAM substrate (Figure 5d−f, right-hand side), an anisotropic topography develops with time. The difference between height profiles averaged along the x direction and those averaged along the y direction are particularly evident at late times (cf. Figure 5f, corresponding to 3060 min). Nevertheless, the line averages along the x direction are identical to the isotropic case, reflecting a statistically homogeneous sample in this direction. The averaged profile $h_y(x)$ in the final state can be fitted with a simple sine wave with a periodicity of 3.9 ± 0.1 μm,[48] consistent with the SAM pattern period. The time evolution of the line-averaged pattern profile $h_y(x)$ for the 60 nm film, illustrated in Figure 6, presents a more detailed evolution of the surface structure. The presence

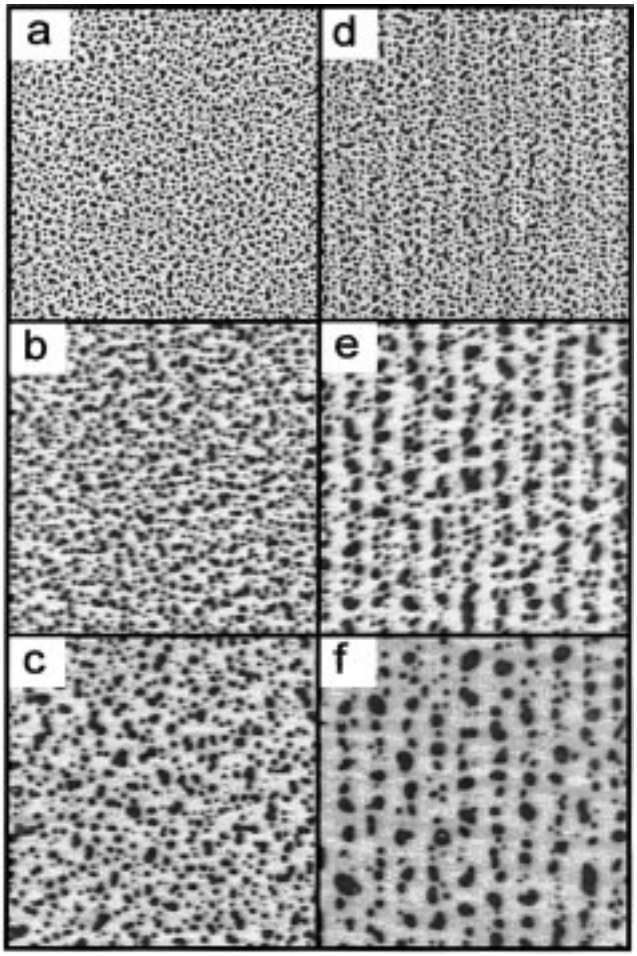

Figure 3. Comparison of morphology evolution for 100 nm thick dPS/PB film on chemically homogeneous and heterogeneous SAM, with the left-hand side representative of samples on homogeneous area and the right-hand side representative of samples on stripe-patterned area. All AFM images are 40 μm × 40 μm with dark regions corresponding to lower features and bright regions corresponding to higher features. Homogeneous substrate: (a) 450, (b) 2010 , and (c) 3100 min; heterogeneous substrate: (d) 420, (e) 2070, and (f) 3060 min.

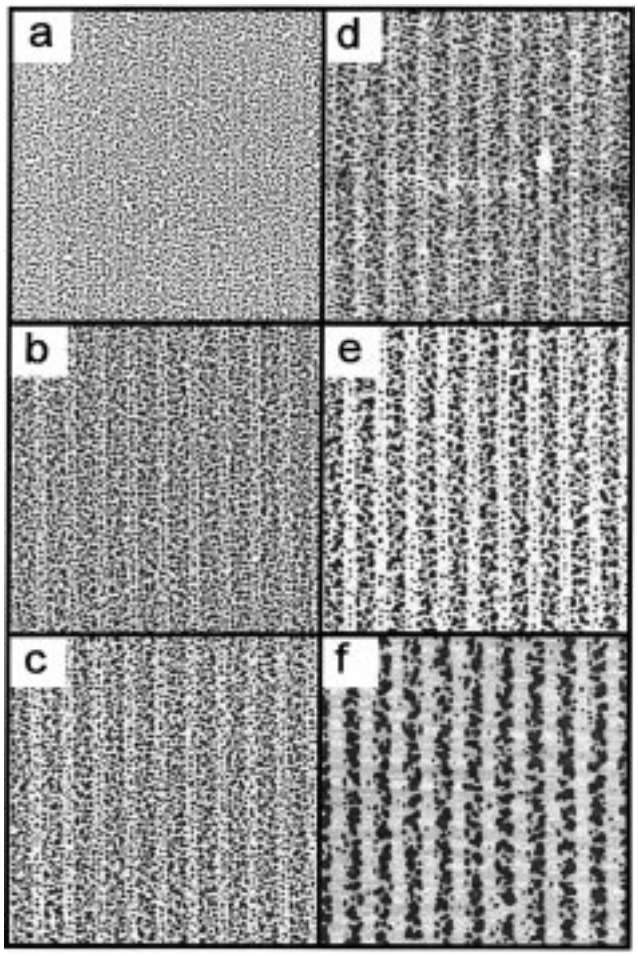

Figure 4. Morphology evolution for 60 nm thick dPS/PB film on stripe-patterned SAM substrate. All images are 40 μm × 40 μm AFM scans of the same sample after (a) 30, (b) 180, (c) 270, (d) 390, (e) 540, and (d) 1380 min.

of the stripe pattern is detectable even at early times (~30 min after spin casting), as shown in Figure 6b in which sharp height variations are found in the *y*-averaged data (open symbols). At intermediate times (e.g., Figure 6c−e), the presence of "double peaks" (local maxima in the height profiles) is clearly visible. This behavior is *qualitatively* different from a progressive onset of a sine wave pattern with a periodicity corresponding to the modulation of the surface energy imposed by the substrate. The occurrence of these local maxima implies that the ordering process involves more than a superposition of a sine wave height modulation and an isotropic phase separation pattern. A more quantitative analysis is necessary to characterize the coarsening and long-range ordering phenomena as discussed in sections C and D.

(C) Height Autocorrelation Analysis. Figure 7 illustrates an example of the evolution of the autocorrelation functions for 60 nm sample for three characteristic times corresponding to early, intermediate, and late times after spin cast. The height autocorrelation function $C(x)$ along the x direction is defined as

$$C(x) = \langle \langle H(X+x,y)\, H(X,y) \rangle_x / \langle H(X) \rangle_x^2 \rangle_y \qquad (1)$$

where $\langle\ \rangle_x$ denotes an average along the x axis and $\langle\ \rangle_y$ denotes an average on the ensemble of the lines constituting each AFM image. Following this definition, $C(x)$ decays to 1 for sufficiently long distances when no long-range correlations are present. The ensemble-averaged autocorrelation functions for the 400 × 400 pixel images were calculated in real space according to eq 1. The height autocorrelation functions $C(x)$ reflected the superposition of two components: a periodic, long wavelength contribution arising from the surface modulation matching the SAM pattern and short scale random height fluctuations. To quantify the correlation length associated with the random height undulations, we then subtracted the periodic component having a periodicity L_0 set by the SAM pattern,

$$\Delta C(x) = C(x) - C_0(x) \qquad (2)$$

$$C_0(x) = A \cos(2\pi x/L_0) \qquad (3)$$

where A is a constant. We found that the value of L_0 in our fits of $C(x)$ based on eqs 2 and 3 coincided with the SAM pattern periodicity within the experimental accuracy. Solid lines are fits to the data following (2) and (3). The inset in Figure 7 shows that $\Delta C(x)$ decays uniformly for the film pattern at late stage where the fluid segregation to the stripes is well developed. The scale of the height fluctuations is determined by the substrate pattern, and this situation is similar math-

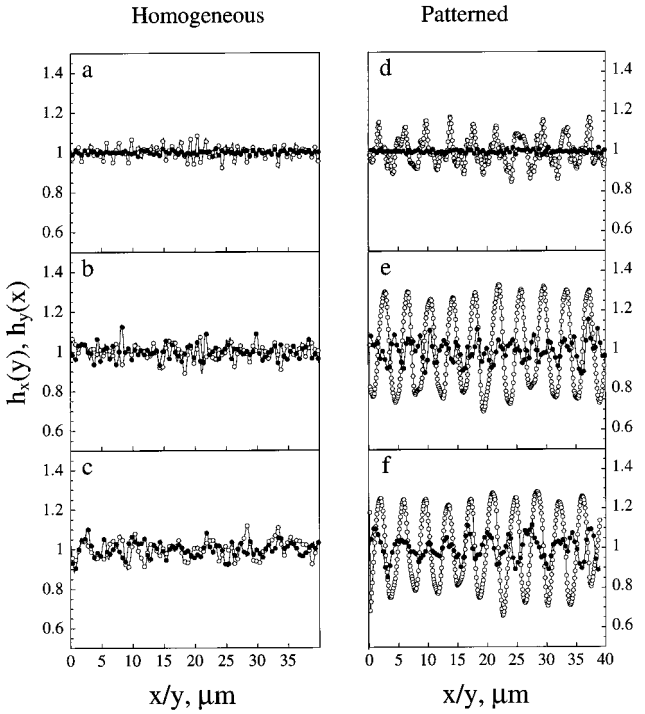

Figure 5. Evolution of the averaged height profiles *h* along the *x* (●) and *y* (○) directions (see text) for the 100 nm film. The 400 data points in each series are joined by continuous lines. For clarity and presentation only a portion of the data points is displayed. Error bars are smaller than symbol size and are not displayed. The left-hand side represents sample on homogeneous area, and the right-hand side represents sample on stripe-patterned area. Homogeneous substrate: (a) 450, (b) 2010, and (c) 3100 min; heterogeneous substrate: (d) 420, (e) 2070, and (f) 3060 min.

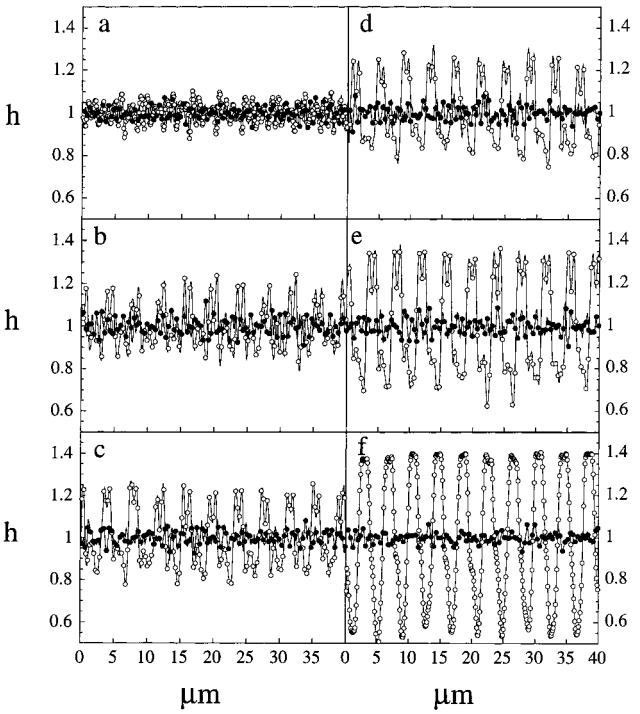

Figure 6. Evolution of the averaged height profiles *h* (see text) along the *x* (●) and *y* (○) directions (see text). The 400 data points in each series of data are joined by continuous lines. For clarity and presentation only a portion of the data points is displayed. Error bars are smaller than symbol size and are not displayed. Film thickness is 60 nm. The data represent the evolution of the pattern after (a) 30, (b) 180, (c) 270, (d) 390, (e) 540, and (d) 1380 min.

ematically to the problem of describing composition fluctuations occurring about a fixed (average) scale. This situation arises, for example, in microemulsions[49−51] and block copolymers in which microphase separation takes place so that composition fluctuations occur about a scale set by the phase separation pattern.[37] In this case, it is possible to model the pair distribution function for the concentration fluctuations phenomenologically as the product of a sinusoidal function multiplied by the pair distribution function so that the composition fluctuations occur about the average microphase separation scale. It is natural to apply the same strategy to $\Delta C(x)$ for the height correlation data. We take $\Delta C(x)$ to equal

$$\Delta C(x) = B \cos(2\pi x/L) \exp(-x/\xi) \qquad (4)$$

where ξ is the correlation length and L is the SAM pattern period. The inset in Figure 7 shows fits of $\Delta C(x)$-data for an early and late time after spin coating (30 and 1380 min, respectively). At all pattern formation stages, we find this form fits the data satisfactorily. From these fits we obtain $\xi(t)$, which provides a measure of the average size of the coarsening phase separation pattern (cf. Figure 10a). The real space analysis of the AFM images reveals some unexpected features that can be further understood by performing a Fourier transform analysis of the data.

(D) FFT Analysis of Film Patterns. Reciprocal space analysis was performed by fast Fourier transformation of 256 × 256 sections of 400 × 400 AFM data arrays. To compare the spectra of different AFM images, each data set was normalized to the average film height.

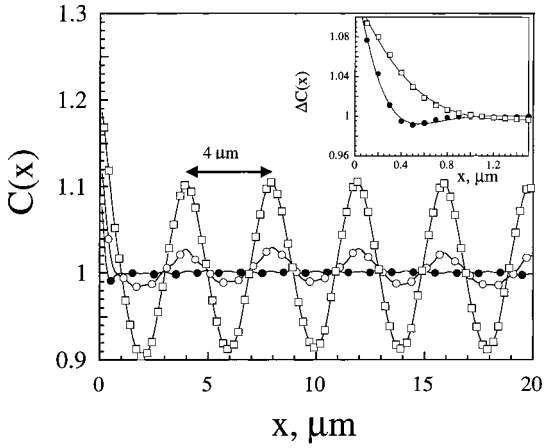

Figure 7. Time evolution of the autocorrelation functions $C(x)$ of the AFM profiles for the 60 nm film on stripe-patterned substrate (see text). Symbols represent delay times of (●) 30, (○) 390, and (□) 1380 min. For clarity purposes only a portion of the 200 data points, which are joined by a solid line, is displayed with a symbol. The inset shows the corrected correlation function $\Delta C(x)$ after 30 (●) and 1380 min (□). The solid lines in the inset are fits to the data using $\Delta C(x) = B \cos(2\pi x/L) \exp(-x/\xi)$ (see text). Error bars are smaller than symbol size and are not displayed for clarity.

Radial averages of the squared amplitudes were calculated to yield the power spectra $P(k)$. In Figure 8 we show a typical result of the fast Fourier transform (FFT) of an AFM image (100 nm film on stripe-patterned substrate after 60 min). In the case of a spun cast sample on a homogeneous SAM, all the FFT spectra show a diffuse, isotropic ring. The samples that are spun cast on stripe-patterned substrates are characterized by

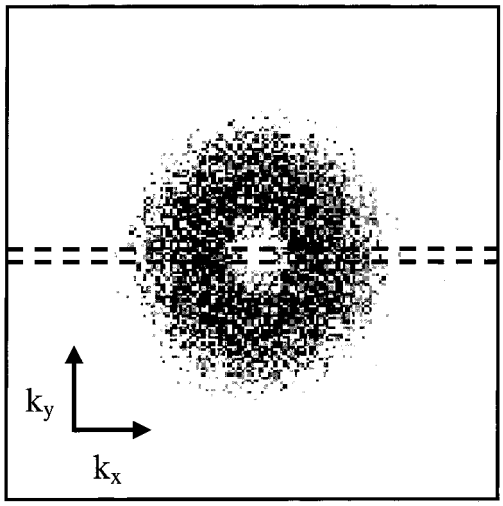

Figure 8. Example of fast Fourier transform of AFM data for 100 nm film on stripe-patterned SAM 60 mm after spin-coating. Dashed lines indicate areas included in the two kinds of averages (see text).

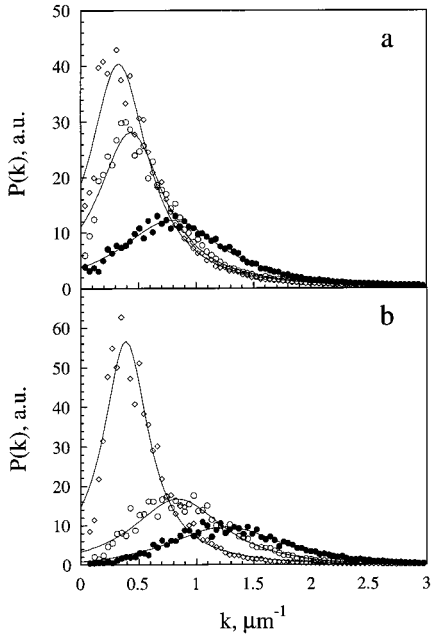

Figure 9. Power spectra, $P(k)$, obtained from radial averages of FFT data for three representative times. Part a shows data for 100 nm thick dPS/PB blend film on homogeneous SAM pattern after (●) 450, (○) 2040, and (◇) 3090 min. Part b shows data for 60 nm thick dPS/PB blend film on stripe-patterned SAM after (●) 30, (○) 270, and (◇) 1410 min. Solid lines are Lorentzian function fits to the data.

two features: a diffuse ring and a series of sharp peaks uniformly distributed along the horizontal axis. These peaks are only 1−3 pixels wide and therefore not visible in Figure 8. To separate these two features, we performed two types of averages. Radial averages of the FFT data lying outside of the central sector (indicated schematically by dotted lines in Figure 8) were performed to characterize the diffuse ring. Sector averages of the FFT data lying inside the central sector were performed to extract the sharp correlation peaks present along the horizontal direction. The size of the central sector (4 pixels) was chosen to optimize the resolution of the peaks.

It is clear from the AFM images (cf. Figures 4 and 5) that the scale of the observed surface structures grows

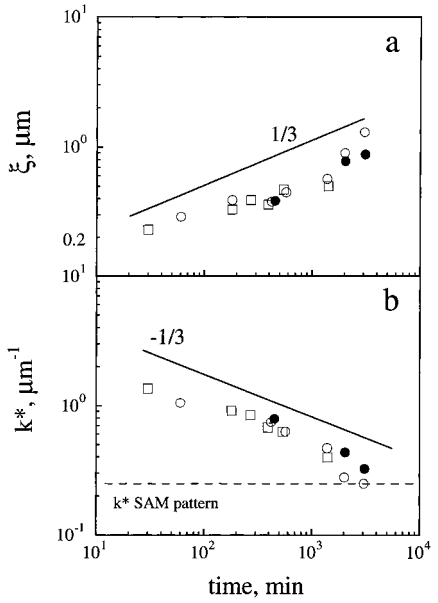

Figure 10. Phase separation coarsening of the polymer blend film.Part a shows the evolution of the correlation length ξ as a function of time on a double-logarithmic plot for three different systems. Symbols represent (●) 100 nm blend film on homogeneous substrate, (○) 100 nm film on patterned substrate, and (□) 60 nm film on patterned substrate. Part b represents the position of k^*, determined from the Lorentzian fits to the data, as a function of time on a log−log plot. The symbols are the same as in part a. Solid lines represent slopes of 1/3 and are plotted for comparison.

with time. In Fourier space, the same trend is illustrated by the two-dimensional ring shifting toward lower k values, where k denotes spatial frequency. The wavevector magnitude for which the intensity of the diffuse FFT ring is maximum is noted k^*. The diffuse ring is qualitatively similar in all the FFT, being isotropic for the films on the homogeneous as well as the stripe-patterned substrates (not shown). In the case of the thicker films the stripe-patterned substrate does not induce any observable symmetry breaking for the structures giving rise to the diffuse ring, at least for the thicker films. In Figure 9 we display the evolution of radially averaged power spectra $P(k)$ for a 100 nm film on an homogeneous substrate (Figure 9a) and for a 60 nm film on a stripe-patterned substrate (Figure 9b). The time evolution of the power spectra is not affected by the presence of the stripe pattern, and observations on the 100 nm film on a stripe-patterned substrate (not shown) are similar. The radially averaged data can be fit adequately with a shifted Lorentzian:

$$P(k) = a + b/[(k - k^*)^2 + c] \quad (5)$$

where a, b, and c are free fitting parameters. This functional form was useful to determine systematically k^* for the different samples.[52]

In Figure 10 we show a comparison of the time evolution of ξ (Figure 10a) and of k^* (Figure 10b) for the thicker films studied. The time evolutions of ξ and k^* are well described by a 1/3 power law, indicated by the solid line in both plots. We note that the results of both real space (autocorrelation function) and Fourier analysis are consistent. The characteristic correlation length scale ξ (or equivalently k^{*-1}) is not strongly dependent on the chemical homogeneity of the substrate or film thickness, at least in the 100 nm thickness range.

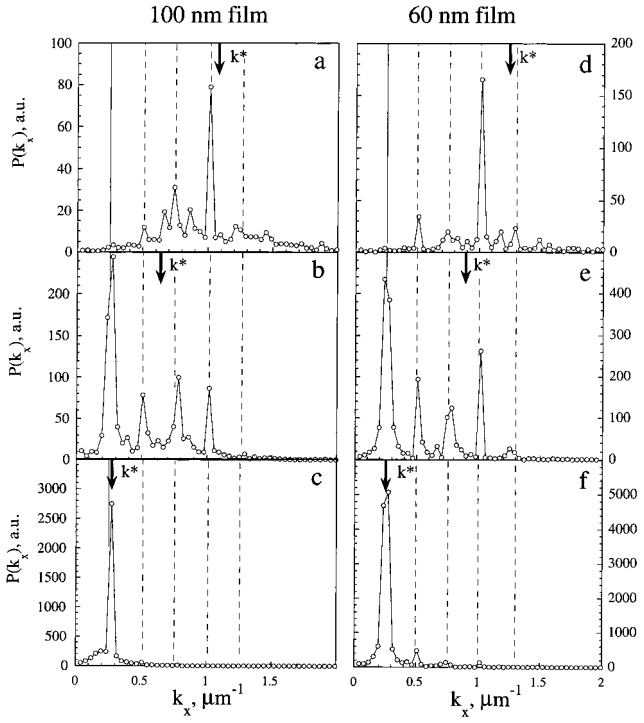

Figure 11. Horizontal central sector power spectrum, $P(k_x)$, obtained by averaging a narrow horizontal section of the 2-D FFT transform data showing the time evolution of the harmonic peaks for several representative times. Plots on the left-hand side represent data for the 100 nm film on a stripe-patterned area for (a) 60, (b) 570, and (c) 3060 min. Plots on the right-hand-side represent data for the 60 nm film on a stripe-patterned area for (d) 30, (e) 270, and (f) 1410 min. The position of the phase separation wavevector k^* (see Figure 8) for each time interval is depicted by the arrows.

The horizontal dashed line in Figure 10b represents the position of wavevector associated with the stripe periodicity of the SAM pattern. Figure 10b shows that the progressive coarsening of the isotropic component of the film topography reaches a maximum when its length scale becomes comparable to the pattern size.

The occurrence of phase separation in self-organizing thin polymer films was invoked in previous works;[10,11] however, no kinetic evidence supporting this interpretation was provided. The 1/3 scaling of the correlation length is commonly found in the early stages of film phase separation in bulk. The scaling behavior of this growth process is characteristic of spinodal decomposition, Ostwald ripening, or diffusive coalescence. It is therefore difficult to ascribe a definite mechanism of the coarsening, beyond the observation that it reflects phase separation.[44]

We next focus our attention on the anisotropic structure associated with the development of the stripe pattern. In Figure 11 we show the evolution of the FFT power spectra averaged in the central narrow horizontal portion of the transformed data, for the 60 and 100 nm film at three representative times. The arrows depict the corresponding positions of k^* from Figure 9. In both cases several sharp peaks are evident. The value of k_1 in Figure 11a−f coincides with the inverse of the measured periodicity of the SAM pattern; namely, we find that $k_1 = k_{SAM} = 0.25\ \mu m^{-1}$ in all the transform data sets. The positions of the higher frequency peaks are integer multiples of the fundamental spatial frequency. The positions of k_{SAM} and the calculated harmonic frequencies (i.e., $k_n = nk_{SAM}$, where n is an integer) are represented on Figure 11 by vertical solid and dashed lines, respectively. By comparing Figures 3d, 5d, and 11a, which correspond to various presentations of the same data, we see that the higher harmonics are associated with the sharp variations of the film height profiles. In addition, the longer the sample is allowed to equilibrate, the more its topographic profile approaches a simple sine wave, which corresponds to a single peak in Fourier space. In other words, these higher order harmonics in Fourier space do not result from transforms of "square wave" profiles.

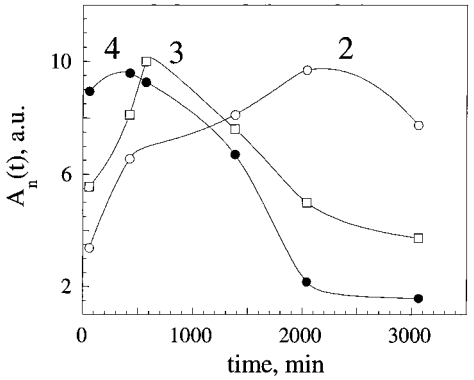

Figure 12. Time evolution of the harmonic mode amplitudes $A_i(t)$ with $i > 1$. Solid lines are guides to the eye.

While the intensities of the harmonic peaks vary with time, their positions are dictated by the stripe geometry and are insensitive to the phase separation coarsening process. Both samples display the same behavior, namely the amplitude of fundamental mode increases monotonically with time, whereas the higher harmonics reach a maximum and then decay progressively. The behavior of the amplitudes of the higher order harmonic modes [$A_n(t)$, with $n > 1$] is summarized in Figure 12. It can be seen that the amplitudes of the $n > 1$ modes increase at early times and decrease at long times, whereas the fundamental increases monotonically. Figure 12 also indicates that the intensity for the higher modes reaches a maximum when k^* (depicted by arrows in Figure 11) coincides with k_n and then decrease as k^* becomes smaller. These observations indicate that the phase separation and the ordering processes are coupled. The data in Figure 12 can be interpreted as implying that the phase separation process excites the surface deformation modes when the scale of the phase separation pattern k^* becomes commensurate with the harmonic frequencies, k_n. Remarkably, this "resonance" between phase separation and surface deformation occurs even at early times when the characteristic size of the phase separation morphology is much smaller than the stripe periodicity. The *amplitude* A_1, associated with the fundamental mode, is directly related to the amplitude of the long-range height modulation of the surface and, thus, representative of the degree of film ordering imposed by the underlying SAM stripe pattern. Therefore, the time evolution of A_1 provides a means to quantify the ordering kinetics of the blend films. The ordering kinetics for two film thicknesses in terms of A_1 is illustrated in Figure 13, where the data are fit to the expression

$$A_1(t) = A_{\infty,1}[1 - \exp(-t/\tau)] \qquad (6)$$

$A_{\infty,1}$ is the limiting peak amplitude of the fundamental, and τ is the characteristic time constant for the ordering

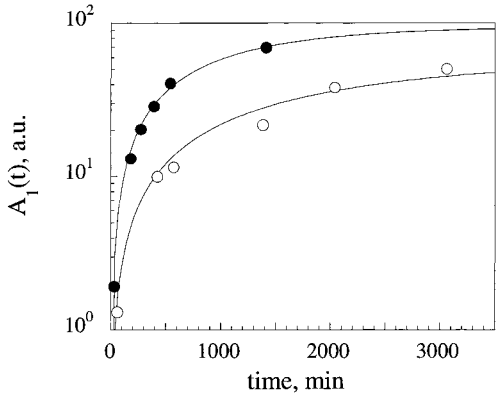

Figure 13. Time evolution of the amplitude associated with the fundamental mode, k_1. The solid lines are fits to the data using $A_1(t) = A_{\infty,1}[1 - \exp(-t/\tau)]$, where $A_{\infty,1}$ is the limiting peak amplitude of the fundamental and τ is the characteristic time constant for the ordering process. Error bars are smaller than symbol size and are not displayed for clarity.

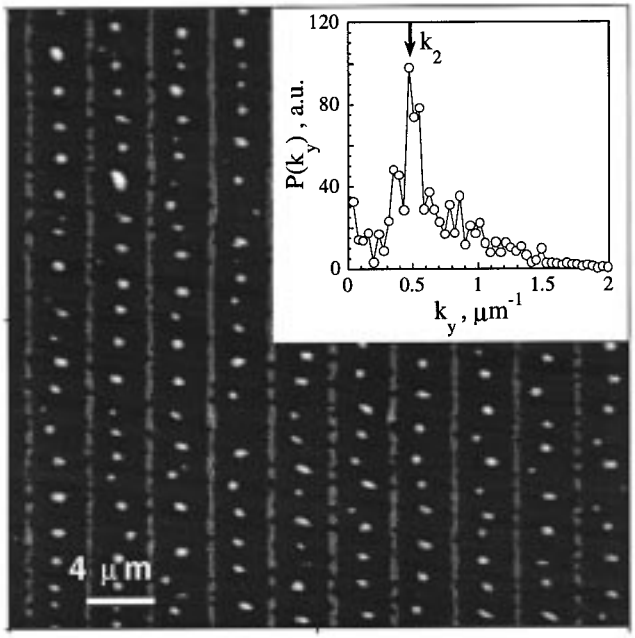

Figure 14. AFM image corresponding to Figure 2d. Bright regions correspond to high features. The inset shows the power spectrum resulting from vertical sector averaging of the FFT. The position of the maximum, k_2, corresponds to half the stripe-pattern period (see text).

process. Equation 6 assumes that the kinetics occurs by a first-order rate process and that A_1 vanishes at short times and approaches a constant at long times.[53] This functional form fit the data satisfactorily and allowed the determination of the time constants $\tau =$ 1100 min for the 60 nm film and $\tau = 2200$ min for the 100 nm film. The faster ordering process for the thinner film most likely reflects the diminishing influence of the substrate on the surface morphology as film thickness increases.[54]

Another feature of ultrathin polymer films was observed, namely the tendency of the polymer stripes to break up, as in the 20 nm thick sample shown in Figure 14 (note that Figure 14 is an alternative representation of Figure 2d). In this sample we see that the polymer stripe patterns are replaced by arrays of fairly uniformly spaced droplets, separated by continuous lines. The inset in Figure 14 shows the power spectrum obtained by averaging the FFT transform of an AFM image in a central vertical sector (6 pixels wide). In this case, the position of the maximum coincides with k_2, which corresponds to the double of the fundamental frequency of the SAM pattern. Moreover, the periodicity revealed by the inset is this time along the y direction (parallel to the stripes) and corresponds to half the stripe pattern period. Recent studies[30] have shown that thin polystyrene films (less than 10 nm thick) spontaneously break up through thermally excited capillary waves. These thermally induced film instabilities can be expected to occur more readily in stringlike structures because of the increased degrees of freedom for deformation. We suggest that the phenomenon illustrated in Figure 14 has its origin in the breakup of fluid "threads" on the surface by capillary instability, as normally observed in late stage phase separation in the bulk and in blend films on unpatterned substrates.[22] In our case it seems very likely that the thinner films undergo phase separation, but instead of reaching the same conformation as the thicker films, the fluid "threads" are then broken up by a capillary instability. The uniformity of the droplet size supports this hypothesis.

In this view, the fluctuations in the fluid boundary due to thermal energy limit the scale at which surface patterns can be resolved. These observations strongly suggest that fine polymer structures having dimensions on the order of a few tens of nanometers should be unstable to thermal fluctuations. This instability should be useful, however, in applications where fine, uniform droplet dispersions on interfaces are desirable.

4. Conclusion

We presented AFM data for the phase separation of a polymer blend film on SAM substrate. By real-space and Fourier analysis of the AFM data, we provide evidence that the predominant cause of coarsening is phase separation. Although phase separation drives the organization of the film, there is an interaction of this process with the fluid segregation driven by the presence of a SAM pattern on the film substrate. A coupling between phase separation and the surface deformation modes is observed in which the phase separation process excites surfaces modes of a commensurate scale. These modes decay after further coarsening occurs, and lower frequency surface deformation modes become excited. The problem of fluid phase separation on a patterned substrate provides an ideal geometry for studying the coupling of surface deformation modes and phase separation that are important for many processes involving ultrathin polymer films.

We also identify a fundamental limitation in the use of phase separation as means to achieve formation of polymer patterns: spontaneous thermal fluctuations tend to destroy these small structures. We must then seek some means (e.g., entanglements, cross-linking, electrostatic interactions) of reducing the effects of these fluctuations in order to create more stable structures at the nanometer scale.

Acknowledgment. We are grateful to John A. Rogers of Lucent Technologies for providing the SAM patterned substrates and to Professor J. W. Mays of the University of Alabama, Birmingham, for providing the deuterated poly(styrene) used in these measurements. We also thank Ben P. Lee for fruitful discussions and Eric J. Amis for his helpful comments.

References and Notes

(1) Wu, S. *Polymer Interface and Adhesion*; Marcel Dekker: New York, 1982.
(2) Prime, K. L.; Whitesides, G. M. *Science* **1991**, *252*, 1164.
(3) Rockel, H.; Huber, J.; Gleiter, R.; Schuhmann, W. *Adv. Mater.* **1994**, *6*, 568.
(4) Licari, J. J.; Hughes, L. A. *Handbook of Polymer Coatings for Electronics: Chemistry, Technology, and Applications*; Noyes Publications: Park Ridge, NJ, 1990.
(5) Cowie, J. M. G. *Polymers: Chemistry and Physics of Modern Materials*; Chapman and Hall: New York, 1991.
(6) Netz, R. R.; Andelman, D. *Phys. Rev. E* **1997**, *55*, 687.
(7) Onda, T.; Shibuichi, S.; Satoh, N. *Langmuir* **1996**, *12*, 2125.
(8) Service, R. F. *Science* **1997**, *278*, 383.
(9) Krausch, G.; Kramer, E. J.; Rafailovich, M. H.; Sokolov, J. *Appl. Phys. Lett.* **1994**, *64*, 2655.
(10) Karim, A.; Douglas, J. F.; Lee, B. P.; Glotzer, S. C.; Rogers, J. A.; Jackman, R. J.; Amis, E. J.; Whitesides, G. M. *Phys. Rev. E* **1998**, *57*, R 6273.
(11) Böltau, M.; Walheim, S.; Mlynek, J.; Krausch, G.; Steiner, U. *Nature* **1998**, *391*, 877.
(12) Jones, R. A. L.; Norton, L. J.; Kramer, E. J.; Bates, F. S.; Wiltzius, P. *Phys. Rev. Lett.* **1991**, *66*, 1326.
(13) Krausch, G.; Dai, C. A.; Kramer, E. J.; Bates, F. S. *Ber. Bunsen-Ges. Phys. Chem.* **1994**, *98*, 446.
(14) Bruder, F.; Brenn, R. *Phys. Rev. Lett.* **1992**, *69*, 624.
(15) Krausch, G.; Dai, C. A.; Kramer, E. J.; Bates, F. S. *Phys. Rev. Lett.* **1993**, *71*, 3669.
(16) Krausch, G.; Dai, C. A.; Kramer, E. J.; Marko, J. F.; Bates, F. S. *Macromolecules* **1993**, *26*, 5566.
(17) Ball, R. C.; Essery, R. L. H. *J. Phys.: Condens. Matter* **1990**, *3*, 10303.
(18) Marko, J. F. *Phys. Rev. E* **1993**, *48*, 2861.
(19) Puri, S.; Frisch, H. L. *J. Phys.: Condens. Matter* **1997**, *9*, 2109.
(20) Glotzer, S. C. *Annu. Rev. Comput. Phys.* **1995**, *2*, 1.
(21) Chen, H.; Chakrabarti, A. *Phys. Rev. E* **1997**, *55*, 5680.
(22) Sung, L.; Karim, A.; Douglas, J. F.; Han, C. C. *Phys. Rev. Lett.* **1996**, *76*, 4368.
(23) Karim, A.; Slawecki, T. M.; Kumar, S. K.; Douglas, J. F.; Satija, S. K.; Han, C. C.; Russell, T. P.; Liu, Y.; Overney, R.; Sokolov, O.; Rafailovich, M. H. *Macromolecules* **1998**, *31*, 857. It is also important for the films to be in the weak segregation regime in order to avoid complications due to the coupling of phase separation, spin casting, and solvent evaporation.
(24) Ermi, B. D.; Karim, A.; Douglas, J. F. *J. Polym. Sci., Part B: Polym. Phys.* **1998**, *36*, 191.
(25) Mayes, A. M.; Kumar, S. K. *MRS Bull.* **1997**, *22*, 43.
(26) Vrij, A. *Discuss. Faraday Soc.* **1966**, *42*, 23.
(27) Brochard, F.; Daillant, J. *Can. J. Phys.* **1990**, *68*, 1084.
(28) Young, C. Y.; Clark, N. A. *J. Chem. Phys.* **1981**, *74*, 4184.
(29) Reiter, G. *Phys. Rev. Lett.* **1992**, *68*, 75.
(30) Xie, R.; Karim, A.; Douglas, J. F.; Han, C. C.; Weiss, R. A. *Phys. Rev. Lett.* **1998**, *81*, 1251. In relatively thick films the energetic cost of nucleating holes can become prohibitive so that the film should remain smooth beyond another characteristic length.
(31) Leibler, S. *J. Phys. (Paris)* **1986**, *47*, 507.
(32) Leibler, S.; Andelman, D. *J. Phys. (Paris)* **1987**, *48*, 2013.
(33) Marder, M.; Frisch, H. L.; Langer, J. S.; McConnell, H. M. *Proc. Natl. Acad. Sci. U.S.A.* **1984**, *81*, 6559.
(34) Gebhardt, C.; Gruler, H.; Sackmann, E. *Z. Naturforsch.* **1977**, *32C*, 581.
(35) Seul, M.; Andelman, D. *Science* **1995**, *267*, 476.
(36) Kawakatsu, T.; Andelman, D.; Kawasaki, K.; Taniguchi, T. *J. Phys. II* **1993**, *3*, 971.
(37) Bates, F. S.; Fredrickson, G. H. *Annu. Rev. Phys. Chem.* **1990**, *41*, 525.
(38) Taniguchi, T. *Phys. Rev. Lett.* **1996**, *16*, 4444.
(39) Lamb, H. *Hydrodynamics*; Dover Publications: New York, 1983.
(40) Miles, J. W. *Proc. R. Soc. London* **1967**, *A297*, 459.
(41) Ermi, B. D.; Nisato, G.; Douglas, J. F.; Karim, A. *Phys. Rev. Lett.* **1998**, *81*, 3900.
(42) According to ISO 31-8, the term "molecular weight" has been replaced with "relative molecular mass", symbol Mr. The conventional notation, rather than the ISO notation, has been employed for this publication.
(43) Kumar, A.; Biebuyck, H. A.; Whitesides, G. M. *Langmuir* **1994**, *10*, 1498.
(44) Sung, L. P.; Han, C. C. *J. Polym. Sci., Part B: Polym. Phys.* **1995**, *33*, 2405.
(45) Gruell, H. Personal communication.
(46) The reference to commercial equipment or supplies does not imply its recommendation or endorsement by the National Institute of Standards and Technology.
(47) The standard uncertainty is calculated from the width of the FFT.
(48) The standard uncertainty is calculated from the goodness of the fits.
(49) Teubner, M.; Strey, R. *J. Chem. Phys.* **1987**, *87*, 3195.
(50) Schubert, K. V.; Strey, R.; Kline, S. R. *J. Chem. Phys.* **1994**, 5343.
(51) Hoylst, R.; Schick, M. *J. Chem. Phys.* **1992**, *96*, 7728.
(52) k^* for the different samples was determined with a standard uncertainty of $\pm 0.01\ \mu m^{-1}$.
(53) Douglas, J. F.; Johnson, H. E.; Granick, S. *Science* **1993**, *262*, 2010.
(54) Robbins, M. O.; Andelman, D.; Joanny, J.-F. *Phys. Rev. A* **1991**, *43*, 4344.

MA981546X